J Solid State Electrochem (2012) 16:227–234
DOI 10.1007/s10008-011-1315-x

ORIGINAL PAPER

An aqueous rechargeable lithium-ion battery based on $LiCoO_2$ nanoparticles cathode and LiV_3O_8 nanosheets anode

Hossein Yadegari · Ali Jabbari · Hossein Heli

Received: 6 November 2010 / Revised: 8 January 2011 / Accepted: 14 January 2011 / Published online: 8 February 2011

Abstract Nanoparticles of lithium cobalt oxide ($LiCoO_2$) and nanosheets of lithium vanadium oxide (LiV_3O_8) were synthesized by a citrate sol–gel combustion route. The physical characterizations of the electrodic materials were carried out by scanning electron microscopy (SEM), transmission electron microscopy (TEM), and also X-ray diffraction (XRD) measurements. Near spherical nanoparticles of ≈100 nm and compact nanosheets with a few nanometers thick were observed by SEM and TEM for $LiCoO_2$ and LiV_3O_8, respectively. XRD data indicated that the as-prepared active materials presented pure phase of rhombohedral $LiCoO_2$ with R-3m symmetry and monoclinic LiV_3O_8 with $p2_1/m$ symmetry. The kinetics of electrochemical intercalation of lithium ion into the nanoparticles of $LiCoO_2$ and nanosheets of LiV_3O_8 from 1.0 mol l^{-1} $LiNO_3$ aqueous solution were investigated by cyclic voltammetry and chronoamperometry. An aqueous rechargeable lithium-ion battery consisting of $LiCoO_2$ nanoparticles as positive and LiV_3O_8 nanosheets as negative electrode was assembled. This battery represented a discharge voltage of about 1 V with good cycling performance.

H. Yadegari · A. Jabbari (✉)
Department of Chemistry, K. N. Toosi University of Technology,
P.O. Box 16315-1618, Tehran, Iran
e-mail: jabbari@kntu.ac.ir

H. Heli
Laboratory of Analytical and Physical Electrochemistry,
Department of Chemistry, Science and Research Branch,
Islamic Azad University,
Fars, Iran

H. Heli
Young Researchers Club, Science and Research Branch,
Islamic Azad University,
Fars, Iran

Keywords Lithium · Intercalation · $LiCoO_2$ · LiV_3O_8 · Kinetic analysis · Aqueous rechargeable lithium-ion battery

Introduction

Secondary lithium-ion batteries are modern power sources for portable electronic devices such as cellular phones, notebook computers, and camcorders due to their high specific energy, high voltage, flexible and lightweight design, and long shelf-life. However, the conventional lithium-ion batteries contain flammable organic electrolytes, which cause these lithium-ion batteries to be relatively expensive in consequence of special cell designing, the indispensability of a perfectly dry environment during manufacturing steps, and the costly organic electrolytes [1]. Besides, the conductivities of organic electrolytes are typically two orders of magnitude lower than that of an aqueous system, which limits the rate capability and specific power. On the other hand, formation of a solid electrolyte interphase passivation layer at the electrode/electrolyte interface, because of irreversible side reactions that occur at the interface between the electrode and electrolyte, is known to lead to capacity fade in lithium-ion cells [2]. As a result, lithium-ion batteries with aqueous solution electrolytes have many advantages such as low cost, easy manufacturing, intrinsic safety, and environmental friendly [1, 3–6].

The first type of rechargeable lithium-ion batteries with aqueous electrolyte was introduced by Li et al. [3–5]. Subsequntly, spinel $Li_2Mn_4O_9$ or $Li_4Mn_5O_{12}$ anode and $LiMn_2O_4$ cathode materials were used to assemble aqueous lithium-ion batteries [7]. Recently, the hybrid energy-storage cells using $LiMn_2O_4$, $LiCoO_2$, and $LiCo_{1/3}Ni_{1/3}Mn_{1/3}O_2$ as positive electrodes and activated carbon as

negative electrode with aqueous electrolyte have been proposed [8–10]. Other types of rechargeable lithium-ion batteries with a pair of metal oxides (LiV_3O_8 as anode and $LiCoO_2$ and $LiMn_2O_4$ as cathode materials) were also reported by Wang et al. [11, 12]. At the same time, another research group has tried to improve the cycling performance of lithium-ion cell $LiMn_2O_4/Li_xV_2O_5$ with aqueous solution electrolyte by polypyrrole coating on the anode [13]. More recently, Liu et al. have developed a rechargeable aqueous lithium-ion battery using olivine $LiMn_{0.05}Ni_{0.05}Fe_{0.9}PO_4$ as cathode and NASICON $LiTi_2(PO_4)_3$ as anode materials [14]. Moreover, MnO_2, $LiMnPO_4$, and $LiFePO_4$ cathode materials [15–19] and TiO_2, TiP_2O_7, $LiTi_2(PO_4)_3$, and LiV_3O_8 anode materials [1, 20–24] for storage devices based on the lithium-ion intercalation/deintercalation in aqueous electrolytes were also employed.

There is no doubt at this time that the nano-scaled materials provide short diffusion pathway for lithium ion insertion/extraction from host materials and simultaneously expose high specific surface areas which often provide more active intercalation sites [25, 26]. The recent most advanced studies of lithium-intercalated materials take care of nano-scaled compounds for application in aqueous and non-aqueous lithium-ion batteries [20, 21, 27]. In the study presented here, the nanoparticles of $LiCoO_2$ and nanosheets of LiV_3O_8 were synthesized via citrate assisted sol–gel method. Applying solution preparative techniques such as sol–gel process to synthesis of chemical compounds allow a better mixing of the elements than solid-state mixing and thus enable the synthesis of a purer material. On the other hand, lower reaction temperature and shorter reaction time are then possible to yield a compound of high homogeneity and high surface area. Moreover, citrate (in the present case) can act either as fuel and oxidant in the synthesis mixture and also can decrease the particles size of the synthesized compound by releasing the combustion gases during the calcination process. The intercalation properties of the synthesized oxides as cathode and anode materials for aqueous rechargeable lithium-ion battery (ARLB) were investigated. Subsequently, the electrochemical performance of an ARLB based on $LiCoO_2$ nanoparticles as the positive electrode, LiV_3O_8 nanosheets as the negative electrode, and an aqueous $LiNO_3$ solution as the electrolyte were also examined.

Materials and methods

Materials

All chemicals were of analytical grade from Merck and were used without further purification. All solutions were prepared with doubly distilled water.

Synthesis of nanoparticles of $LiCoO_2$

Nanoparticles of $LiCoO_2$ were synthesized by a citrate sol–gel method. The synthesis process is briefly described as follows: stoichiometric amount of lithium acetate and cobalt (II) acetate were mixed in distilled water and a solution of citric acid anhydrous was added to the mixture under constant magnetic stirring. The ratio of the total amount of metal ions to citric acid was 1:1. The obtained mixture was evaporated at 80 °C for 8 h until conversion to a polymeric resin. Afterward, the obtained polymeric resin was further dried in an oven at 120 °C overnight to remove the excess water. The remaining solid mass was ground and then calcined at 500 °C for 10 h to obtain nanoparticles of $LiCoO_2$.

Synthesis of nanosheets of LiV_3O_8

Nanosheets of LiV_3O_8 were synthesized by a similar citrate assisted sol–gel method as follows: stoichiometric amount of lithium oxalate ($Li_2C_2O_4$) and vanadium (V) oxide (V_2O_5) were mixed in distilled water and a solution of citric acid anhydrous was added to the mixture under constant magnetic stirring. The ratio of the total amount of metal ions to citric acid was 1:1. V_2O_5 was slightly solved in water and the color of glum yellow appeared in the mixture. Then the pH of the solution was adjusted to 7.0 by adding ammonia solution. In this pH V_2O_5 was solved completely and the solution color changed to transparent dirt yellow. The obtained mixture was evaporated at 80 °C for several hours. The color of the solution turned to light green and then to the dark blue. Afterward, the obtained blue gel was further dried overnight in an oven at 120 °C to remove the excess water. Finally, the blue solid mass was ground and then calcined at 450 °C for 20 h to obtain the nanosheets of LiV_3O_8.

Electrode preparation

In order to prepare the working electrode for the electrochemical experiments, the $LiCoO_2$ nanoparticles or LiV_3O_8 nanosheets (80%) was ground with polyvinylidene difluoride (10%) and acetylene black (10%) and dispersed in *N*-methyl pyrrolidone by means of an ultrasonic bath to obtain a paste. The resulting composites were supported on 2.0 mm diameter Pt disk electrodes and then heated to 100 °C in an oven for several hours. The working electrodes contained ≈0.2 mg of the active materials. The electrochemical behavior of the electrodes was studied in a conventional three-electrode cell with a Pt plate and an Ag/AgCl, 3 M KCl as the counter and reference electrodes, respectively. The supporting electrolyte was a solution of 1.0 M $LiNO_3$.

Apparatus

Electrochemical measurements were carried out in a conventional three-electrode cell containing 1.0 M $LiNO_3$ solution powered by a μ-Autolab potentiostat/galvanostat, type III (The Netherlands). The system was run by a PC through GPES 4.9 softwares.

Surface morphological studies were carried out using a Model X-30 Philips scanning electron microscope (SEM). The transmission electron microscopy (TEM) was performed using a CEM 902A ZEISS transmission electron microscope, with an accelerating voltage of 80 kV. Samples were prepared by placing a drop of the particles, dispersed in acetone, on a carbon-covered copper grid (400 mesh) and evaporating the solvent.

Powder X-ray diffraction (XRD) patterns were measured by a Philips X'Pert (The Netherlands) using Cu Kα radiation at 40 kV and 30 mA in the 2θ range from 10° to 70°.

Results and discussion

Morphological characterization

SEM micrographs of the as-prepared $LiCoO_2$ and LiV_3O_8 samples with different magnifications are depicted in Fig. 1. The $LiCoO_2$ images (Fig. 1a) represent particles with an average size of less than 100 nm. The particle size of LiV_3O_8 (Fig. 1b) in the first look is in the range of several micrometers. However, closer look on the particles indicates a layered structure for the LiV_3O_8 sample. The LiV_3O_8 particles consisted of packed layers of LiV_3O_8 with a few nanometers thick. TEM technique with inherently higher resolution was applied for more morphological investigation of the synthesized materials. TEM micrographs of the as-prepared $LiCoO_2$ and LiV_3O_8 are shown in Fig. 2. Spherical particles with 100 nm diameter are seen in Fig. 2a, while a layered structure with a few nanometers thick is observed in Fig. 2b. The layered configuration for the LiV_3O_8 sample caused parallel orientation of lithium ion diffusion pathway which increases the diffusion process efficiency.

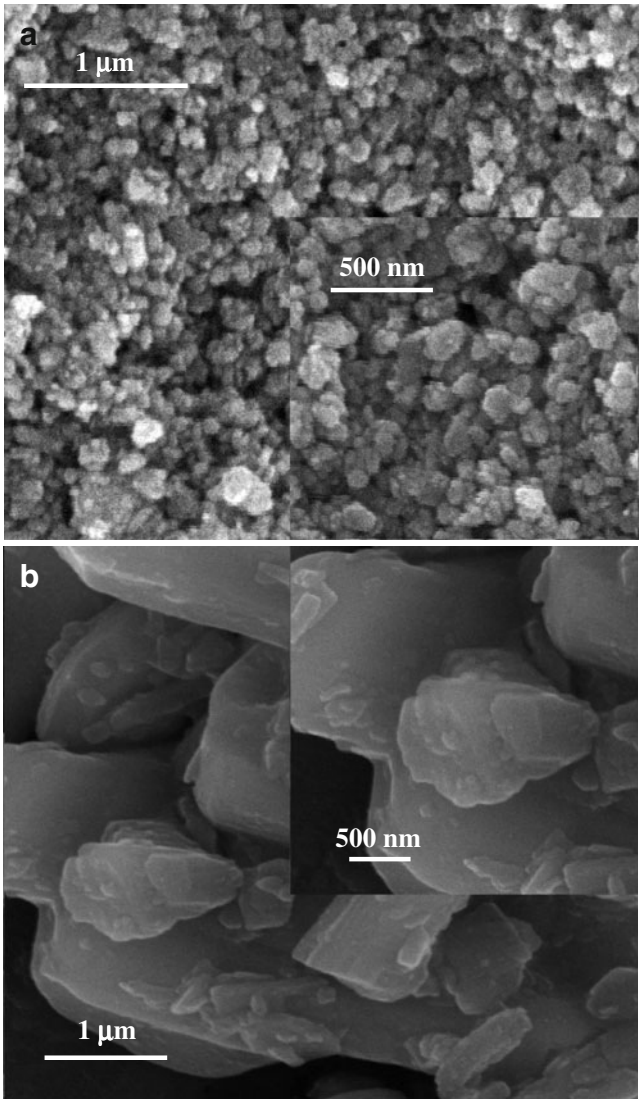

Fig. 1 SEM images of $LiCoO_2$ nanoparticles (**a**) and LiV_3O_8 nanosheets (**b**) with two magnifications

Structural investigation

X-ray diffraction patterns were employed to characterize the phase structure of the as-prepared $LiCoO_2$ nanoparticles and LiV_3O_8 nanosheets. Typical powder XRD patterns of the synthesized materials are shown in Fig. 3. The $LiCoO_2$ pattern contains slightly broadened peaks, due to the nanometer-size effect [28]. The nanoparticles are randomly oriented polycrystalline with main diffraction peaks at 2θ values of 18.9, 37.4, and 45.3 correspond to (0 0 3), (1 0 1), and (1 0 4) diffractions, respectively. The peaks can be identified with those for a rhombohedral $LiCoO_2$ structure with R-3m space group (No. 166) [29]. The LiV_3O_8 pattern contains obvious diffraction lines in the XRD pattern of LiV_3O_8 which all can be indexed to a monoclinic system with $p2_1/m$ space group [30]. The peak at about $2\theta = 13.9°$ is assigned to the diffraction at the (1 0 0) plane indicating the layered structure of LiV_3O_8. Moreover, the relative intensity of the crystal plane (1 0 0) is lower than that have been reported for preferential ordered crystals of LiV_3O_8. This indicate that the preferential ordering which would lead to a long path for Li^+ ion diffusion and is not beneficial to intercalation process is avoided in the synthesized LiV_3O_8 nanosheets [31–33]. The XRD data suggests that the LiV_3O_8 nanosheets have appropriate orientation of

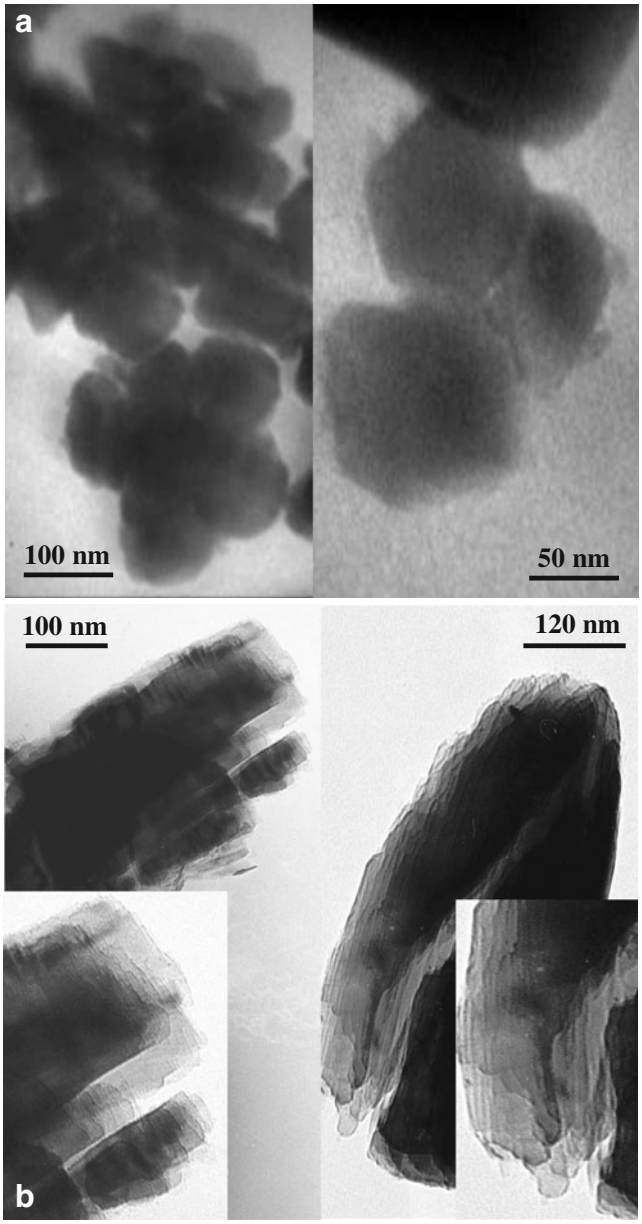

Fig. 2 TEM micrographs of $LiCoO_2$ nanoparticles (**a**) and LiV_3O_8 nanosheets (**b**) with two magnifications

lithium ion diffusion pathways which is advantageous for intercalation/deintercalation process of lithium ion. In addition, the calculated lattice parameters are as a=6.68 Å, b=3.60 Å, c=12.03 Å, and V=275.40 Å^3 for LiV_3O_8 nanosheets and a=2.82 Å, c=14.04 Å, c/a=4.98, and V=96.49 Å^3 for $LiCoO_2$ nanoparticles.

Electrochemical behavior

Typical cyclic voltammograms of the $LiCoO_2$ nanoparticles and LiV_3O_8 nanosheets recorded in 1.0 M $LiNO_3$ solution using a potential sweep rate of 0.3 mV s^{-1} are shown in

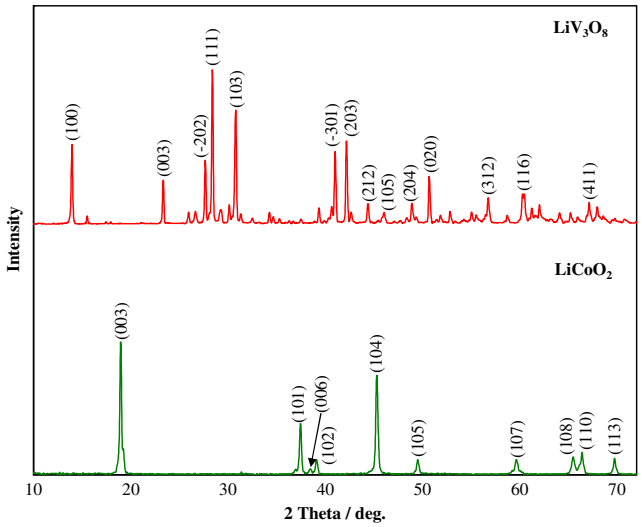

Fig. 3 Typical X-ray diffraction patterns of the $LiCoO_2$ nanoparticles and LiV_3O_8 nanosheets

Fig. 4. One pair of sharp and quite reversible redox peaks are observed in both voltammograms owning to the insertion and extraction of lithium ion into the host materials. The mid-peak potentials are 757 and −268 mV for $LiCoO_2$ nanoparticles and LiV_3O_8 nanosheets, respectively. The mid-peak potentials have a potential difference of more than 1000 mV so it can be applied as cathode and anode in an aqueous lithium-ion battery.

Cyclic voltammograms of the $LiCoO_2$ nanoparticles and LiV_3O_8 nanosheets in 1.0 M $LiNO_3$ solution recorded at different potential sweep rates in the range of 2 to 40 mV s^{-1} for $LiCoO_2$ and 2 to 80 mV s^{-1} for LiV_3O_8 are shown in Fig. 5. Upon increasing the potential sweep rate, the height and area of both redox peaks increase, while the corresponding charges (related to the electrode capacity) remain almost unchanged. This manner confirms the

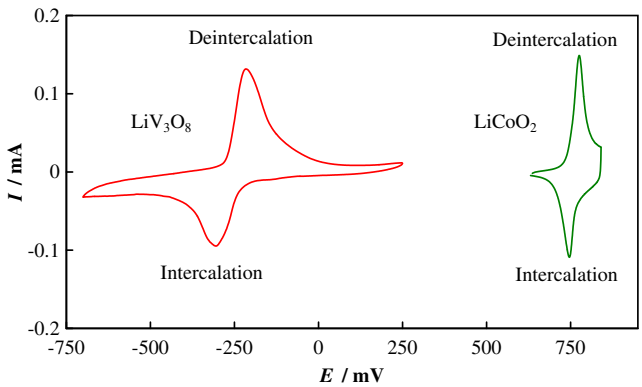

Fig. 4 Typical cyclic voltammograms of $LiCoO_2$ nanoparticles and LiV_3O_8 nanosheets recorded in 1.0 M $LiNO_3$ solution. The potential sweep rate was 0.3 mV s^{-1}

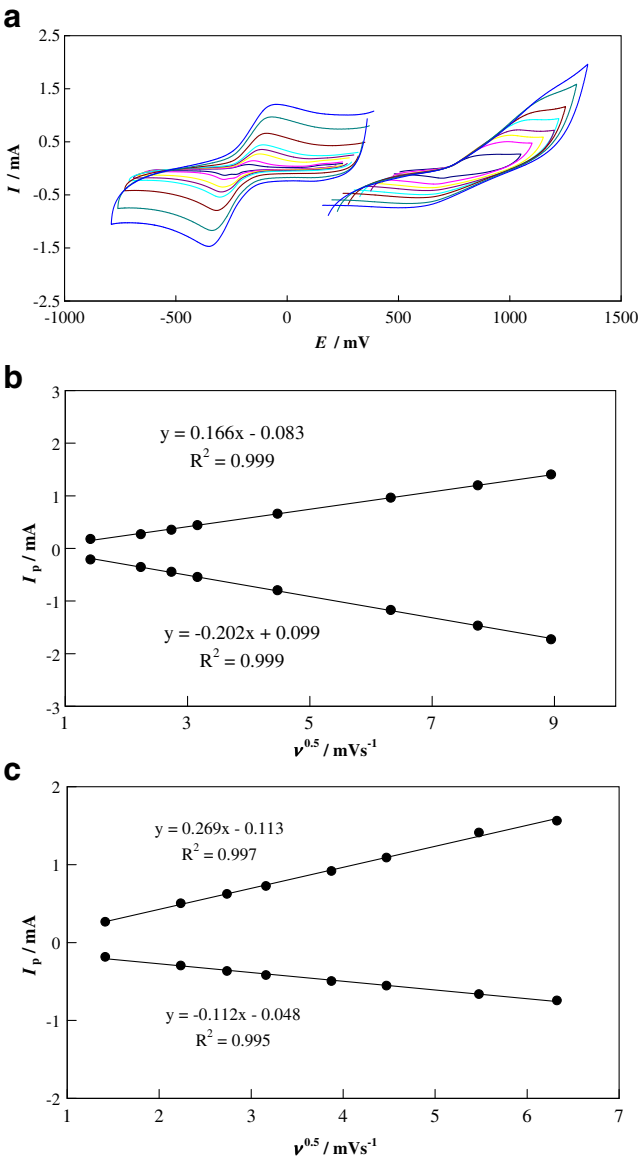

Fig. 5 **a** Cyclic voltammograms of the $LiCoO_2$ nanoparticles and LiV_3O_8 nanosheets in 1.0 M $LiNO_3$ solution recorded at different potential sweep rates (the potential sweep rates from the inner to the outer was: 2, 5, 7.5, 10, 15, 20, 30, and 40 mV s^{-1} for $LiCoO_2$ nanoparticles and 2, 5, 7.5, 10, 20, 40, 60, and 80 mV s^{-1} for LiV_3O_8 nanosheets). **b** Dependency of the cathodic and anodic peak currents on the square root of the potential sweep rate for LiV_3O_8 nanosheets. **c** Dependency of the cathodic and anodic peak currents on the square root of the potential sweep rate for $LiCoO_2$ nanoparticles

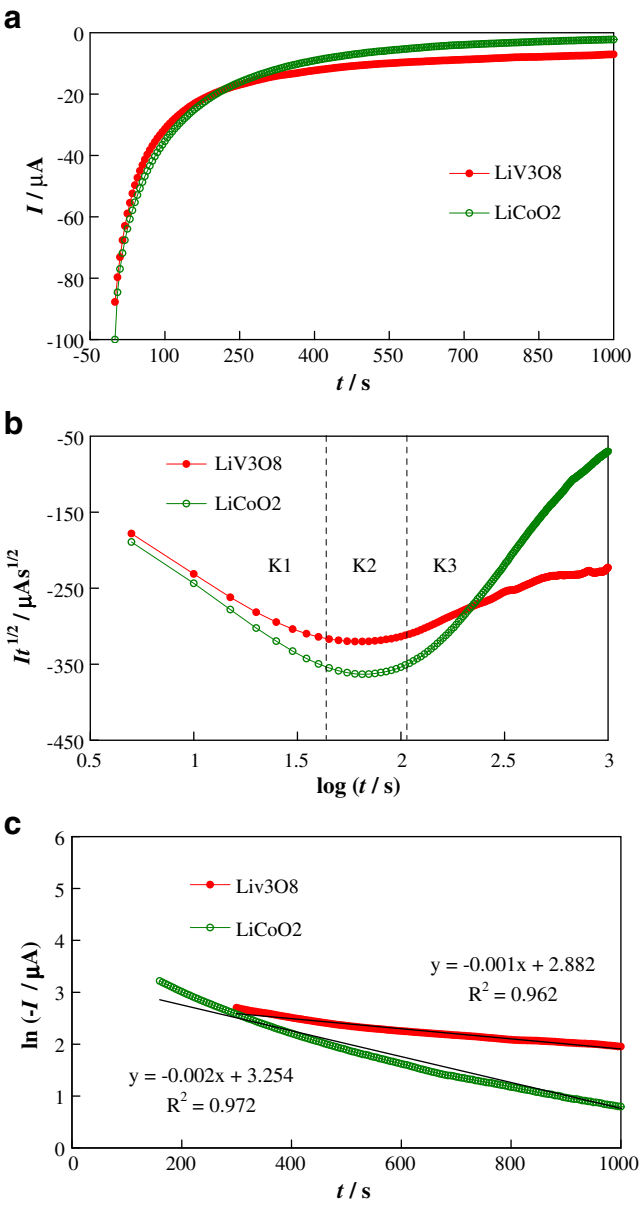

Fig. 6 **a** Typical chronoamperograms of $LiCoO_2$ nanoparticles and LiV_3O_8 nanosheets recorded in 1.0 M $LiNO_3$ solution using a step potential of 740 and −350 mV, respectively. **b** The Cottrell plots correspond to (**a**). **c** ln(*I*) vs. *t* plots

favorable kinetics of charge transfer even at high potential sweep rates. In the case of $LiCoO_2$ nanoparticles, however, it seems that the intercalation process (reduction process) is performed with a lower rate in comparison with the deintercalation process (oxidation process). This may be due to the solvation of lithium ion by water molecules in aqueous electrolytes. Lithium ion must leave the hydrated water molecules before intercalation to the host material. In addition, currents of both anodic and cathodic peaks of the $LiCoO_2$ nanoparticles and LiV_3O_8 nanosheets depend linearly on the square root of the potential sweep rate (Fig. 5b and c). The results indicate that the intercalation/deintercalation processes are controlled via diffusion of lithium ion in the host material.

Chronoamperometry is an operative electrochemical technique for investigation of intercalation process. In a typical chronoamperometry (CA) experiment, the potential of the working electrode is stepped, and the resulting current from faradic processes occurring at the electrode

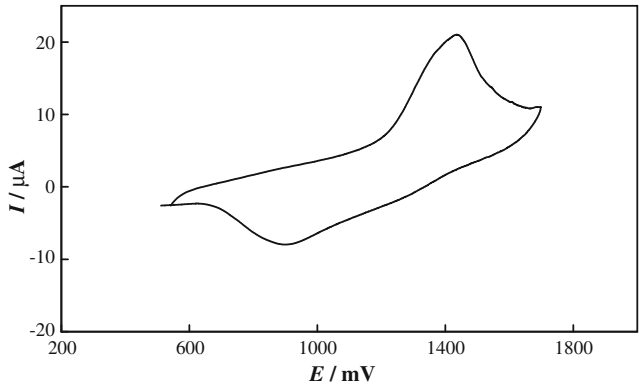

Fig. 7 A typical cyclic voltammogram of the battery system consisting of $LiCoO_2$ nanoparticles as positive and LiV_3O_8 nanosheets as negative electrode recorded in 1.0 M $LiNO_3$ solution. The potential sweep rate was 0.5 mV s^{-1}

(caused by the potential step) is monitored as a function of time until steady-state conditions are achieved. This technique is powerful for the characterization of ion diffusion in the solid state host materials [34, 35]. The expression of the current response to a potential step at a long time domain, assuming one-dimensional diffusion transport of a species under finite-space conditions, can be represented as follows [35]:

$$I(t) = 2\,\Delta Q \Big/ \tau_d \sum_{m=0}^{\infty} \exp\left[-(2m-1)^2\pi^2 t/(4\tau_d)\right] \quad (1)$$

for $t > \tau_d$

where $I(t)$ is the current response to the potential step, ΔQ is the total charge transferred into the electrode during the potential step, τ_d is the diffusion time constant, t is the elapsed time from the beginning of the potential step, and m is an integer number, with:

$$\tau_d = l^2/D_{Li} \quad (2)$$

and

$$\Delta Q = \int_0^{\infty} I(t)\,dt = -F\,A\,l\,\Delta C \quad (3)$$

where l is the diffusion length, F is the Faraday constant, and ΔC is the variation of the diffusing species concentration.

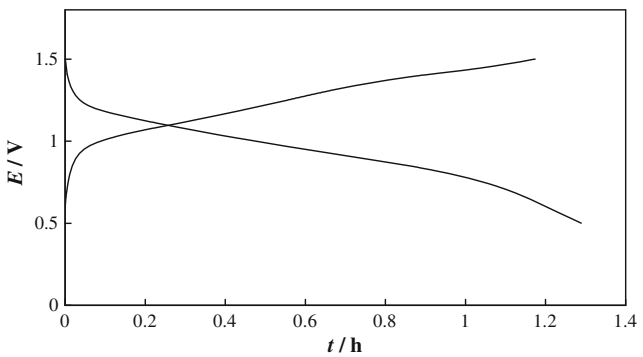

Fig. 8 Typical chronopotentiograms (charge/discharge curves) of the battery system consisting of $LiCoO_2$ nanoparticles and LiV_3O_8 nanosheets as positive and negative electrodes, respectively, in 1.0 M $LiNO_3$ solution in the potential range of 0.5 to 1.5 V at a current density of 0.1 mA cm^{-2}

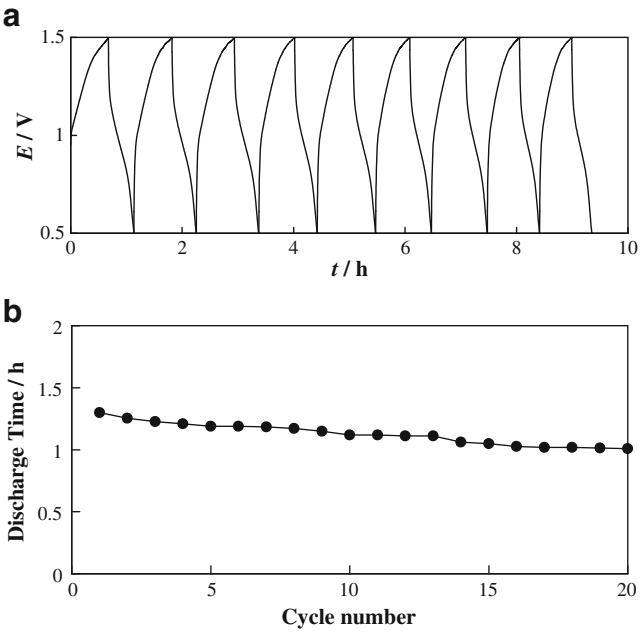

Fig. 9 **a** Ten consecutive charge/discharge curves of the aqueous rechargeable cell. **b** Dependency of the discharge capacity of the cell on the cycle number

In this study, potentials of 740 and −350 mV (correspond to the potentials of the cathodic peaks in the cyclic voltammetry plot, Fig. 4) were enforced to record the chronoamperograms of $LiCoO_2$ nanoparticles and LiV_3O_8 nanosheets, respectively. The results are depicted in Fig. 6a. The net currents are decayed exponentially to a limiting current due to the fact that the mass transport of intercalating species occurred only by diffusion. The corresponding Cottrell plots ($I \times t^{1/2}$ vs. log (t)) are shown in Fig. 6b. In the plots, various time domains of the intercalation process for lithium ion into the $LiCoO_2$ nanoparticles and LiV_3O_8 nanosheets are witnessed. Three different kinetic regions can be distinguished from the plots corresponding to the separate steps of the entire intercalation process. Region K1 (short term) corresponds to the double layer charging and is related to the interfacial charging of both the Pt/active material and the active material/electrolyte interfaces [35, 36]. Region K2 (medium

term) represents almost constant values for the $I \times t^{1/2}$, reflecting that the semi-infinite planar diffusion of lithium ions into the $LiCoO_2$ nanoparticles and LiV_3O_8 nanosheets occurs in this region [35–37].

Region K3 (long term) represents the finite-space diffusion of lithium ion into the active materials in the long time domain [35–37]. Dependency of the response current with time in region K3 can be derived from Eq. 1 and represented by the following equation [36, 38]:

$$I = \left(2\,\Delta Q\, D_{\mathrm{Li}}/l^2\right) \exp\left(-\pi^2 D_{\mathrm{Li}} t/4l^2\right) \quad (4)$$

The plots of ln(I) vs. t which have linear relations for $t>$ 160 s in the case of $LiCoO_2$ and for $t>300$ s in the case of LiV_3O_8 are shown in the Fig. 6c. From the slope of these lines and using Eq. 4, the diffusion coefficients of lithium ion into the $LiCoO_2$ nanoparticles and LiV_3O_8 nanosheets for intercalation process were obtained as 2.26×10^{-10} and 1.89×10^{-10} cm^2 s^{-1}, respectively.

A battery system consisting of $LiCoO_2$ nanoparticles as positive and LiV_3O_8 nanosheets as negative electrode was assembled and tested. Figure 7 shows the first cyclic voltammogram of the battery system in the potential range of 0.5 to 1.8 V recorded in 1.0 M $LiNO_3$ solution using a potential sweep rate of 0.5 mV s^{-1}. One pair of redox peak is clearly seen in the voltammogram corresponding to the charge and discharge processes of the cell according to the following equation:

$$LiCoO_2 + LiV_3O_8 \leftrightarrow Li_{1-x}CoO_2 + Li_{1+x}V_3O_8 \quad (5)$$

Typical charge/discharge curves of the battery system recorded at a current density of 0.1 mA cm^{-2} are depicted in Fig. 8. In addition, Ten consecutive charge/discharge curves of the battery are shown in the Fig. 9a. It can be seen that the battery shows the similar charge and discharge curves, reflecting the good reversibility and performance of the battery. Moreover, Fig. 9b shows the discharge capacity of the cell versus cycle number. The curve shows that the cell retains the 80% of the initial capacity after 20 cycles.

Conclusion

Nanoparticles of $LiCoO_2$ and nanosheets of LiV_3O_8 were prepared by a new process using citrate as fuel and metal acetates as the source of metal ions. The electron microscopy investigations indicated that the prepared active materials have spherical shape with mean diameter of about 100 nm in the case of the cathode and compact nanosheets with a few nanometers thick in the case of anode materials. Structural analysis using X-ray powder diffraction showed that the synthesized $LiCoO_2$ nanoparticles and LiV_3O_8 nanosheets were of good crystallinity which was confirmed with electrochemical experiments. The kinetic parameters of the intercalation were studied by means of cyclic voltammetry and potential step chronoamperometry. Lithium ion diffusion coefficients were determined by analyzing the data of the CA measurements. An aqueous rechargeable lithium-ion battery based on the nanoparticles of $LiCoO_2$ as positive and nanosheets of LiV_3O_8 as negative electrode has been constructed with 1 mol l^{-1} $LiNO_3$ solution as electrolyte. This battery showed discharge voltage of about 1 V with good cycleability.

Acknowledgement The financial support of the Iran National Science Foundation (INSF) is gratefully acknowledged. The Research Councils of K. N. Toosi University of Technology, Islamic Azad University and young Researchers Club are also gratefully acknowledged.

References

1. Köhler J, Makihara H, Uegaito H, Inoue H, Toki M (2000) Electrochim Acta 46:59–65
2. Kostecki R, Kong F, Matsuo Y, McLarnon F (1999) Electrochim Acta 45:225–233
3. Li W, Dahn JR, Wainwright DS (1994) Science 264:1115–1118
4. Li W, Mckinnon WR, Dahn JR (1994) J Electrochem Soc 141:2310–2316
5. Li W, Dahn JR (1995) J Electrochem Soc 142:1742–1746
6. Lee JW, Pyun SI (2004) Electrochim Acta 49:753–761
7. Wang GX, Zhong S, Bradhurst DH, Dou SX, Liu HK (1998) J Power Sources 74:198–201
8. Wang YG, Xia YY (2006) J Electrochem Soc 153:A450–A454
9. Wang YG, Luo JY, Wang CX, Xia YY (2006) J Electrochem Soc 153:A1425–A1431
10. Wang YG, Luo JY, Wu W, Wang CX, Xia YY (2007) J Electrochem Soc 154:A228–A234
11. Wang GJ, Zhao NH, Yang LC, Wu YP, Wu HQ, Holze R (2007) Electrochim Acta 52:4911–4915
12. Wang GJ, Zhang HP, Fu LJ, Wang B, Wu YP (2007) Electrochem Commun 9:1873–1876
13. Wang H, Zeng Y, Huang K, Liu S, Chen L (2007) Electrochim Acta 52:5102–5107
14. Liu XH, Saito T, Okada S, Yamaki J (2009) J Power Sources 189:706–710
15. Wu MS, Lee RH (2008) J Power Sources 176:363–368
16. Manickam M, Singh P, Issa TB, Thurgate S, Macro RD (2004) J Power Sources 130:254–259
17. Manickam M, Singh P, Mitchell DRG (2007) J Electrochem Soc 154:A109–A113
18. Minakshi M, Singh P, Thurgate S, Prince K (2006) Electrochem Solid-State Lett 9:A471–A474
19. Manickam M, Singh P, Thurgate S, Prince K (2006) J Power Sources 158:646–649
20. Reiman KH, Brace KM, Gordon-Smith TJ, Nandhakumar I, Attard GS, Owen JR (2006) Electrochem Commun 8:517–522
21. Wu MS, Wang MJ, Jow JJ, Yang WD, Hsieh CY, Tsai HM (2008) J Power Sources 185:1420–1424
22. Wang H, Huang K, Zeng Y, Yang S, Chen L (2007) Electrochim Acta 52:3280–3285

23. Wang GJ, Qu QT, Wang B, Shi Y, Tian S, Wu YP, Holze R (2009) J Power Sources 189:503–506
24. Heli H, Yadegari H, Jabbari A (2011) Mater Chem Phys. doi:10.1016/j.matchemphys.2010.12.057
25. Shaju KM, Jiao F, Debart A, Bruce PG (2007) Phys Chem Chem Phys 9:1837–1842
26. Lou XW, Deng D, Lee JY, Feng J, Archer LA (2008) Adv Mater 20:258–262
27. Bruce PG, Scrosati B, Tarascon JM (2008) Angew Chem Int Ed 47:2930–2946
28. Cullity BD (1978) Elements of X-Ray Diffraction, 2nd edn. Addison-Wesley, Reading
29. Johnston WD, Heikes RR, Sestrich D (1958) J Phys Chem Solids 7:1–13
30. Wadsley AD (1957) Acta Crystallogr 10:261–267
31. Pistoia G, Pasquali M, Wang G, Li L (1990) J Electrochem Soc 137:2365–2370
32. Kawakita J, Kato T, Katayama Y, Miura T, Kishi T (1999) J Power Sources 81–82:448–453
33. Yanga H, Li J, Zhang XG, Jin YI (2008) J Mater Process Tech 207:265–270
34. Bard AJ, Faulkner LR (2001) Electrochemical Methods, 2nd edn. Wiley, New York
35. Levi MD, Aurbach D (1997) J Phys Chem B 101:4641–4647
36. Das SR, Majumder SB, Katiyar RS (2005) J Power Sources 139:261–268
37. Levi MD, Lu Z, Aurbach D (2001) Solid State Ionics 143:309–318
38. Levi MD, Levi EA, Aurbach D (1997) J Electroanal Chem 421:89–97